Interpretation of Aura Satellite Observations of CO and Aerosol Index related to the December 2006 Australia Fires

Mingzhao Luo,[1*] Christopher Boxe,[1] Jonathan H. Jiang,[1] Ray Nassar,[2] and Nathaniel Livesey[1]

[1]Earth and Space Science Division, Jet Propulsion Laboratory, California Institute of Technology, Pasadena, CA, 91109, USA
[2]Centre for Global Change Science, Departmenst of Physics and Geography, University of Toronto, Toronto, ON M5S 1A7, Canada

*****Manuscript Correspondence, e-mail: Ming.Luo@jpl.nasa.gov

Abstract

Enhanced Carbon Monoxide (CO) in the upper troposphere (UT) is shown by collocated Tropospheric Emission Spectrometer (TES) and Microwave Limb Sounder (MLS) measurements near and down-wind from the known wildfire region of SE Australia, December 12th-19th, 2006. Enhanced UV aerosol index (AI) derived from Ozone Monitoring Instrument (OMI) measurements correlate with these high CO concentrations. HYSPLIT model back trajectories trace selected air parcels to the SE Australia fire region from the initial locations with enhanced TES CO in the upper and lower troposphere. Simultaneously, they show a lack of vertical advection along their tracks. TES retrieved CO vertical profiles in the higher and lower southern latitudes are examined together with the averaging kernels and show that TES CO retrievals are most sensitive at approximately 300-400 hPa. The enhanced CO observed by TES at the upper (215 hPa) and lower (681 hPa) troposphere are therefore influenced by mid-tropospheric CO. GEOS-Chem model simulations with an 8-day emissions inventory as the wildfire source over Australia, are sampled to the TES/MLS observation times and locations. These simulations only show CO enhancements in the lower troposphere near and down-wind from the wildfire region of SE Australia with drastic underestimates of UT CO. Although CloudSat along-track ice-water content curtains are examined to see whether possible vertical convection events can explain the high UT CO values, sparse observations of collocated Aura CO and CloudSat along-track ice-water content measurements for the single event precludes any conclusive correlation. Vertical convection that uplift fire-induced CO (*i.e.*, most notably referred to as pyro-cumulonimbus (pyroCb)) is likely responsible for the TES/MLS observations. The PyroCb mechanism is currently not incorporated in GEOS-Chem, thus providing a potential explanation for the incongruence between its simulations and TES/MLS observations of enhanced CO in the UT.

1. Introduction

Apart from being devastating to local ecosystems and economies, biomass burning and wildfires significantly alter air quality on regional to hemispheric scales (van der Werf et al., 2006) and are an important component of the climate system. They are now recognized to be a major contribution to the global emissions of trace gases and aerosols, significantly affecting atmospheric chemistry, degrading air quality, and impacting the radiative transfer in the atmosphere (e.g. Seiler and Crutzen, 1980; Logan et al., 1981; Crutzen and Andrea, 1990; Liousse et al., 1996; Andreae and Merlet, 2001). One of the principal trace gas species produced during biomass burning events is carbon monoxide (CO). CO plays a central role in atmospheric chemistry by acting as a major sink for hydroxyl radicals ($^{\cdot}$OH) and through its role in the production of ozone (O_3). It is produced as a result of incomplete combustion and the oxidation of methane and non-methane hydrocarbons (NMHCs) and is principally removed by reaction with OH. CO is currently regulated by air quality standards worldwide as a major ozone precursor, and it also contributes to climate change through its effect on ozone and methane chemistry. With biomass burning and oxidation of naturally occurring volatile hydrocarbons accounting for nearly 50% of tropospheric CO (Logan et al., 1981; Thompson et al., 1994), monitoring changes in these sources, changes in anthropogenic sources, and subsequent transport are key to assessing the impact on tropospheric chemistry and near-surface air quality. CO's relatively long lifetime (~2 months), makes it an excellent tracer of transport and source variability (Badr and Probert, 1994). Increases in global tropospheric CO from 1970 to the late 1980s has been linked to increasing anthropogenic emissions (Khalil and Rasmussen, 1988; Yurganov et al., 1997). Subsequent studies found that global tropospheric CO abundances leveled off and began to decrease from 1990 to 2000 because of tighter controls on automobile emissions (Novelli et al., 1994; Khalil and Rasmussen, 1994; Bakwin et al., 1994; Parrish et al., 2002). However, several recent studies have postulated possible large-scale increases and variations in biomass burning sources in the hot and dry rural regions due to climate change (Wotawa et al., 2001; Yurganov et al., 2004; Lapina et al., 2006; Kasischke and Turetsky, 2006).

Biomass and wildfire events have been observed both in the tropics and Northern Hemisphere. Often burning for several weeks, they constitute extremely large perturbations (Turquety et al., 2007), which can increase the background level of relatively long-lived species on hemispheric scales and explain most of the interannual variability in the surface observations

(Wotawa et al., 2001; Szopa et al., 2007). In the mid-latitudes, wildfires, mainly accidental or criminal fires, often burn close to inhabited regions, and efforts are deployed to rapidly control them. On average for the 2000-2006 time period, biomass burning contributed to ~ 5 Tg of CO per year in Europe according to the widely used Global Fire Emissions Database (GFED) version 2 (van der Werf et al., 2006). This appears to be small compared to the estimated total of ~ 82 Tg/year emitted by anthropogenic activities in the same region according to the EDGAR 3.2 FT2000 Inventory (Olivier and Berdowski, 2001). However, since more than 70% of the burning occurs between June and September, their impact becomes critical during the summer.

Southern Europe and the Mediterranean basin are regularly affected by forest fires, which can burn thousands of hectares in a few days. During the severe heat wave of the summer of 2003, Portugal experienced its worst fire season ever recorded, burning more than 4210 km^2 of forest. These wildfires emitted a comparable amount of primary pollutants, comparable to the amount produced from anthropogenic activities, resulting in enhanced pollution and radiative forcing over large parts of Europe (Hodzic et al., 2006 and 2007). The summer of 2007 was among the worst fire seasons of the past decades in Europe. The area burned in five main Southern countries (*i.e.*, Greece, France, Spain, Italy, and Portugal) was well above the average over the past 28 years with a total of 5750 km^2 (EFFIS Forest Fires in Europe 2007 Report, 2008). Greece was the most affected as more than 3000 km2 of land were burned (EFFIS Forest Fires in Europe 2007 Report, 2008; Boschetti et al., 2008), destroying several protected natural sites, thousands of buildings and killing 63 people.

Indonesia experienced some of its most severe wildfires in late 2006, which emitted extreme levels of CO (Rinsland et al., 2008; Logan et al., 2008; van der Werf et al., 2008; Yurganov et al., 2008). Although these fires were mainly deliberately set for the purpose of land clearing, the extent to which they were possible is widely recognized as relating to the regional drought induced by El Niño and the positive Indian Ocean Dipole (Field and Shen, 2009; Nassar et al., 2009).

Australia's dry, windy, and hot climate cause it to be prone to wildfires. Bushfires are a regular feature of the summer, and over the past 40 years more than 250 people have been killed in bushfires (http://www.alertnet.org/thenews/newsdesk/SP65484.htm). For instance, during the late Spring season of 2006, fires burned across many of its regions, including Western Australia, Queensland, Cape York Peninsula, New South Wales, and Victoria. Fire hotspots are routinely

measured by several space-borne remote sensors, such as the Along-Track Scanning Radiometer (ATSR, Arino et al., 2007) and the MODerate resolution Imaging Spectroradiometer (MODIS, Justice et al., 2002). These instruments allow a good evaluation of the location of the main fires under satellite overpass. Signatures from biomass burning are some of the main features observed from space (Lamarque et al., 2003; Edwards et al., 2004; Turquety et al., 2007; McMillan et al., 2008; Yurganov et al., 2008), both due to the large CO concentrations resulting from these fires and to the fact that the fire plumes are often rapidly transported toward the free troposphere, where the IR remote sensors are the most sensitive. Some of these lofting events are rapid as expressed by Fromm et al. (2005) and (2006), which may primarily be due to conditions of extreme convection with sufficient energy to efficiently transport a large amount of material from the planetary boundary layer to the UTLS – most notably referred to as pyro-cumulonimbus (pyroCb) eruptions. Guan et al. (2008) recently simulated pyrcoCb events using the NCAR Community Atmosphere Model (CAM) with a plume-rise parameterization scheme to account for CO over Africa and its export during SAFARI 2000. Their CAM simulation with the plume-rise parameterization scheme show a substantial improvement of the agreements between the modeled and aircraft-measured vertical distribution of CO over Southern Africa biomass burning area. They also concluded that the effect of the plume-rise on free tropospheric CO is more important for the source area (*i.e.*, short-distance transport) than for remote areas (*i.e.*, long-distance transport).

Dirksen et al. (2009) recently investigated the December 2006 Australian forest fires using satellite observations from the Ozone Monitoring Instrument (OMI) and the Cloud-Aerosol Lidar and Infrared Pathfinder Satellite Observation (CALIOP spaceborne lidar) and the TM4 chemistry transport model. The intense heat from the fires caused pyro-convective lofting, which injected aerosol particles into the jet stream. Dirksen et al. (2009) track the resulting aerosol plume using Aerosol Absorbing Index (AAI) observations from OMI and found that it circumnavigated the world in 12 days. Using data from both OMI and CALIOP, they also show that the plume resided in the high troposphere at different stages of its evolution. Constrained by OMI O_2-O_2 retrievals, the TM4 (Tracer Model version 4) chemistry transport model was able to mimic the high injection height (10 km or 250 hPa) of the aerosol plume, associated with pyro-convective lofting.

Here, we discuss the enhanced CO concentrations observed by collocated TES and MLS measurements in the upper troposphere and near and down-wind from the known wildfire region of Southeast (SE) Australia, December 12^{th}-19^{th}, 2006, where TES averaging kernels are used to assess the sensitivity of the TES CO retrievals. Enhanced OMI aerosol index (AI) correlated with high CO values are also evaluated. The Hybrid Single Particle Langrangian Integrated Trajectory (HYSPLIT) model is used to verify the source of the measured CO concentrations away from SE Australia. Lastly, we discuss GEOS-Chem simulations of CO with 8-day GFED v2 emissions as the wildfire source over Australia are sampled to the TES/MLS observation time/locations.

2. TES and MLS CO and OMI AI observations of Australia region in Dec 2006

The CO observations from TES and MLS and the UV absorbing aerosol indices (AI) obtained from the OMI instrument on the Aura satellite are examined for the Australia fire dates of December 12^{th}-19^{th}, 2006. TES operates in nadir mode and provides CO volume mixing ratio (VMR) vertical profiles from the surface to the upper troposphere with limited vertical resolution (Beer et al., 2006). MLS operates in limb mode and provides CO VMR vertical profiles at the observation tangents of 2-3 km think layer for ~215 hPa and above (Waters et al., 2006). OMI's AI is a measure of departures of observed UV spectra from the model spectra without aerosol loading, and its magnitude is a good indicator of the aerosol amount in the atmosphere (Torres et al., 2007).

Figure 1 shows the spatially interpolated CO VMR fields at 215 hPa, obtained from TES and MLS data for December 16^{th}-17^{th}, 2006 respectively. Both instruments observe enhanced CO mixing ratios, at almost identical locations, in this upper tropospheric level. These locations are a few hundreds to a couple of thousands kilometers away from the known fire regions of SE Australia. The values of CO VMR are as large as 400 ppbv for TES at 215 hPa near 32^{o} S, 170^{o} W. The MLS CO VMR at 215 hP are twice those of TES, but the MLS CO data values are known to be a factor of two positively biased (Livesey et al., 2007).

CO data from TES at 681 hPa and 215 hPa and MLS at 215 hPa for December 12^{th}-19^{th}, 2006 are examined in the Australia region. Figure 2 shows spatially interpolated TES and MLS CO VMRs. Since TES Global Surveys (GS) are taken along Aura orbits in a one-day-on followed by one-day-off mode, the continually taken MLS data are selected closest to those of TES. The field patterns for TES and MLS CO at 215 hPa are similar for the four GS time periods.

The TES retrieved CO profiles have limited vertical resolution that can be described by the averaging kernels (AK) and the degree of freedom for signal (DOF). Figure 3 shows the mean averaging kernels for the TES CO profiles with CO > 120 ppbv in the two latitude bands of the Australia region. The DOFs for the two latitude bands are 1.4 (27^o S to 43^o S) and 1.0 (49^o S-72^o S), respectively. As described by Rodgers (1998) and Luo et al. (2007), the retrieved CO profile from remote sensing spectra is the combination of the true CO profile, vertically smoothed by the averaging kernel and the contribution from the a priori profile. In cases 49^o S to 72^o S (see Figure 3, right panel), the TES CO retrieved values at 215 and 618 hPa are both influenced heavily by the true CO values at 400-250 hPa and the a priori values at all levels. It is therefore hardly a convincing conclusion that the enhanced CO in the lower troposphere (681 hPa, bottom row in Figure 2) far away from the source region of SE Australia is valid.

The TES operators are applied to the vertical profiles of the MLS CO retrievals shown in Figure 2, top row (Luo et al., 2007). This process treats MLS CO profiles as the 'true' and simulates the profile that the TES process would have retrieved for the same air sampled by MLS. The high CO distributions in these processed MLS maps for Dec 12^{th}-19^{th}, 2006 (top row of Figure 2) show similar patterns to those of TES observed (mid row of Fig 2), indicating that the enhanced CO plumes indeed appear in the upper troposphere away from the SE Australia fire region.

The OMI aerosol indices (AI) for December 11^{th}-19^{th}, 2006 are shown in Figure 4. The large values of this parameter (*e.g.,* greater than 1) are good indicator of the aerosol plumes generated by the biomass burning. Due to its cross track scan, OMI provides better spatial coverage in the data products compared to TES or MLS. Although OMI's AI maps in Figure 4 are not snap shots (*i.e.*, the orbit swath are separated by ~1.5 hr), they clearly tracked the eastward propagations of at least two major fire plumes, starting on December 11^{th} and 14^{th}, respectively. The second event was also described in detail by Dirksen et al (2009) using OMI data and was tracked the aerosol plums for about eight days.

Here we examine the co-located TES/MLS CO observations and the OMI AI data to identify if the chemical tracer CO and aerosol observations on the Aura platform are consistent in describing the fire plume transport events. The coincidences of enhanced CO and AI data are only identified in a small fraction of orbit overpasses in the region. This is due to four factors. First, TES GS observations occur every other day, and the TES and MLS footprints are along the

Aura orbit tracks only. This means that there rare matching opportunities for the CO and AI data. Secondly, OMI AI data does not have vertical information so that the enhanced CO VMRs observed by MLS at 215 hPa do not necessary coincide with large OMI AI values. Third, TES CO profiles in the troposphere have DOF of 1.0 to 1.4, not adequate to resolve the boundary layers from the upper tropospheric layers. Lastly, OMI only takes measurements in the day time. It is therefore hard to explain the matches or mis-matches between the high TES CO and OMI AI values. As an example, Figure 5 shows the simultaneous measurements of OMI AI, MLS CO at 215 hP, and TES CO at 681 and 215 hPa on December 16th, 2006. On this day TES had no daytime measurements to the east of 140^{o} W and no nighttime measurements to the west of 140^{o} W. MLS CO and OMI AI show enhancement in a same daytime orbit (circled on the plots) while TES data is missing.

3. Trajectory analysis of the enhanced CO, CloudSat vertical curtains of IWC

In the previous section, we presented evidence for the long-range transport of CO from TES and MLS and AI from OMI, which originated from the known Australia fires of December, 2006. Since satellite data are sparse in time and location, we ran an air parcel trajectory model that traces back the high CO observations backward in time to confirm where they originated. The HYSPLIT (Hybrid Single Particle Lagrangian Integrated Trajectory) model developed at Air Resources Laboratory (ARL, http://www.arl.noaa.gov/HYSPLIT_info.php) is used for this study. The meteorological data (wind field) are from the GDAS (Global Data Assimilation System, http://wwwt.emc.ncep.noaa.gov/gmb/gdas/) at 3-hourly, 1 degree latitude/longitude archives at ARL.

Figure 6 shows the air parcel trajectories starting from TES observation locations and times in Dec 16th-17th, 2006 for TES CO volume mixing ratios greater than 120 ppbv and 80 ppbv, respectively. Trajectories start at two TES pressure levels representing the lower and upper troposphere, 681 hPa and 215 hPa, respectively, and they are traced back five days and 2.5 days, respectively. MODIS 8-day fire pixels are also marked indicating the fire locations in the time period. Two conclusions can be drawn from the back-trajectories shown in Figure 6. First, the majority of TES enhanced CO air parcels at 215 hPa can be traced back to the SE Australia fire regions in about 2.5 days, which is a strong indication of the origins of these high COs observed by TES in the upper troposphere. At the lower troposphere (681 hPa), however, the air parcels appear to originate from south of the SE Australia region, at a lower speed than those at 300-200

hPa. These trajectory analyses do not support the hypothesis that high CO observed by TES in the lower troposphere, (Figure 2 bottom panel) away from the fire areas, originated from the Australia fires, but naturally, one should place more confidence in the 2.5 day back trajectories, since trajectory reliability rapidly decreases with increasing time spans. As we discussed in Section 2, these high CO observations by TES at 681 hPa are likely due to the vertical smoothing effect in the retrieval processes.

The second feature shown in Figure 6 is that the trajectories starting at either upper or lower tropospheric levels tend to stay on their pressure levels for several days. No drastic vertical transport is displayed in these trajectories driven by the global assimilated wind fields. Vertical convections that uplift air pollutants and aerosols (*e.g.*, pyrocumulonimbus) occurred over the fires must exist to explain the observed enhanced CO values that are transported far away from their source by the wind system in the upper troposphere (Fromm et al. 2005, 2006).

We made an effort to examine the possible supporting observations of vertical profiles of aerosol or clouds in describing this fire and transport event. There was a data gap in CALIPSO in Dec 6-18 2006 (http://www.calipso.larc.nasa.gov/products/lidar/browse_images/show_calendar.php). The CloudSat Ice/Liquid-Water (IWC/LWC) data are available. The CloudSat IWC/LWC is taken from the Level 2B R04 data set [Austin et al., 2009], with a horizontal resolution of 1.7 km along-track and 1.3 km cross-track. The vertical resolution is ~500 m. Both Aura and CloudSat are part of the A-train (Schoeberl and Talabac, 2006) satellite constellation that follows a similar orbit, separated by less than 15 min. However, for the transport in the East-West directions, the two data sets are not correlated well. Figure 7 shows an example backward air parcel trajectory starting from a TES location where a high CO value was observed. We also overlaid CloudSat tracks prior to the TES observation in an attempt to find coincidences between the back trajectory and the CloudSat vertical Ice-Water observations. No intersections are identified between any CloudSat orbit and the TES backward trajectories starting from all the TES high CO value locations from Dec 11^{th}-19^{th}, 2006. Therefore, it is difficult for the sparse satellite observations to comprehensively describe the process of pollutant transport after a fire event.

4. GEOS-Chem model simulation of the event

Figure 8 shows GEOS-Chem model simulations (Bey et al., 2001) of CO sampled at the TES profile footprints and times (within ±1.5 hours) from December 12^{th}-19^{th}, 2006 in the lower

troposphere (681 hPa) and in the mid-to-upper troposphere (215 hPa). The model was run using GEOS-4 meteorological fields gridded to 2°x2.5° horizontal resolution and 30 vertical sigma levels up to 0.01 hPa, with output written every 3 hours. Year-specific biomass burning emissions for this run were from GFEDv2 (van der Werf et al., 2006) with a temporal resolution of 8-days (based on the MODIS fire counts) but with additional CO enhancement in the Indonesian region (Nassar et al., 2009). EDGAR fossil fuel emissions of CO for Australia in the year 2000 (Olivier and Berdowski, 2001) scaled forward to 2002, were used as implemented by van Donkelaar et al. (2008). Not shown here are the model CO profiles with TES operators applied that simulates the TES retrieved profile assuming model CO profiles as the truth (Luo et al., 2006; Logan et al., 2008). These CO values at 681 hPa are lower than those in Figure 8, due to the combined effects of very low CO values in modeled mid-upper troposphere and the TES a priori profiles.

At 681 hPa TES observes high CO concentrations over SE Australia on December 12^{th}-13^{th}, 2006, while moderate CO concentrations are observed at 215 hPa. On December 14^{th}-15^{th} at both altitudes CO is transported SE of Australia. Thereafter (*i.e.*, from December 16^{th}-19^{th}), much higher CO concentrations are observed at 215 hPa compared to 681 hPa. Nassar et al. (2009) also found an underestimate in CO relative to TES in the Indonesia and Indian Ocean region in late 2006 when GFEDv2 emissions were used directly. One probable explanation for this underestimation was the omission of the CO contribution from smoldering fires, which may not be adequately represented in GFEDv2 since it is based on MODIS observations of active fires. Nassar et al. (2009) scaled CO emissions above the GFEDv2 values to account for the smoldering, which resulted in good agreement with TES observations.

Another important factor indicated by the present work may be the contribution due to conditions of extreme convection with sufficient energy to efficiently transport a large amount of material from the planetary boundary layer to the UTLS – most notably referred to as pyro-cumulonimbus (pyroCb) eruptions (Fromm et al., 2005 and 2006). At 215 hPa, GEOS-Chem model simulations under-predict CO concentrations from December 12^{th}-19^{th}, 2006, especially from December 16^{th}-19^{th}, 2006. If the high CO concentrations observed by TES and MLS from December 16^{th}-19^{th}, 2006 are due to pyroCbs, then the lack of congruence between GEOS-Chem simulations and TES/MLS observations (*i.e.*, the drastic underestimation of CO by GEOS-Chem at 215 hPa) is not surprising as GEOS-Chem does not account for pyroCbs. Despite a slight

underestimation, GEOS-Chem simulates TES CO observations well from December 12th-17th, 2006, but overestimates the amount of CO over SE Australia and underestimates the amount of CO transported SE of Australia on from December 18th-19th, 2006.

Constrained by OMI O_2-O_2 and AAI retrievals, Dirksen et al. (2009) used the TM4 chemistry transport model was used to investigate the height and subsequent transport of the biomass burning plume during the December Australian forest fires, by releasing a passive, but water soluble, tracer in TM4. They conducted simulations with tracer emissions at the surface level (1013 hPa) and at 540 hPa, which resulted in similar tracer vertical distributions with highest tracer concentrations between 300 and 400 hPa. This result suggests that TM4 can, to some degree, simulate the lofting of the plume by the cold front, but also that the model fails to push the plume towards altitudes where it is picked up by the jet stream and where it actually been observed. Dirksen et al. (2009) note that the TM4 is likely deficient as it does not account for the enhanced buoyancy of the plume provided by the heat of the extensive fires. To better simulate the effects of pyro-convection, Dirksen et al. (2009) released the tracer at 248 hPa, which resulted in tracer plumes that are higher by 2-5 km and closer to the observed CALIOP plume altitudes. Again, extreme lofting by pyro-convection, although rare, is important because of the rapid pathway it offers for biomass combustion products to reach the upper troposphere or lower stratosphere (Fromm et al., 2005). Yet, similar to GEOS-Chem, the TM4 model does not incorporate pyroCbs. As pointed out by Hyer et al. (2007), most CTMs do not treat lofting of fire plumes properly and the common way to do so in CTMs studying forest fire events is to impose an injection height as Dirksen et al. (2009). The injection height of emission plumes varies considerably amongst fires, and the lofting of fire emissions depends on the energy of the fire and the local meteorological conditions (Hye er al., 2007). Therefore, CTMs that release emissions of forest fires at pre-defined or fixed injection heights may overlook other causes that can contribute to the existence of a plume at a particular height. Therefore, an appropriate parameterization of the lofting is needed, which needs to account for vegetation type to estimate the heat flux and information on the fire size to calculate the buoyancy flux (Freitas et al., 2007). A 1-D model plume-rise model, adapted from Freitas et al. (2007), currently in development to be implemented in GEOS-Chem, suggests that aerosols emitted from large fires on December 14th, 2006 reached the upper troposphere (~ 380 hPa), in agreement with the OMI O_2-O_2 pressure of the aerosol plume retrieved on that day. This simulation produces an injection height lower

than the TM4 simulations. The difference in injection height indicate that, apart from pyro-convection, another process contributed to the lofting, such as absorbing aerosols known to be subject to considerable heating (*e.g.*, up to 80 W m^{-2}, Stammes et al., 2009).

5. Conclusions

In this paper we presented Aura satellite observations of the enhanced chemical tracer CO (TES and MLS instruments) and the aerosol indices (OMI instrument) in regions down-wind from the Australian fires in December, 2006. We also examined the tracer pathways via the HYSLPLIT trajectory model powered by GDAS wind fields that trace the enhanced CO air parcels back to the known fire sources in the upper troposphere. The trajectories stayed on the upper tropospheric pressure level for 2-3 days between the fire origins and the observation locations. These observations and analyses suggest that for this particular event, the fire generated tracer CO and aerosols in the smoke were uplifted to the mid-upper-troposphere at the fire sources via pyro-convection mechanism suggested previously (Fromm et al., 2005 and 2006) and carried away by the strong horizontal wind system in the upper troposphere.

The TES enhanced CO retrievals in the lower troposphere can be traced back to the general area to the south of the fire origins with a slower air movement compared to the upper troposphere. We examined the vertical information in the TES CO profile retrievals. The DOF are 1.4 and 1.0 for those TES CO profiles between 27^o S to 43^o S and 49^o S to 72^o S, respectively. The TES averaging kernels, which describe the contributions of the true CO profile to the retrieved value, at a given pressure level, peak around 300 hPa. TES reported high CO values in the lower troposphere away from the fire sources are, therefore, partially due to the enhancement in CO in the mid-upper troposphere.

The GEOS-Chem model simulations of tropospheric CO using GFEDv2 biomass burning emissions are examined by extracting model data along TES observation footprints and times. Without the mechanisms that strongly uplift the fire produced CO and aerosols into the upper troposphere, no CO enhancements in model simulations are shown in the upper troposphere compared to the background values. Model CO fields in the lower troposphere do show the production and the transport of high CO values at and away from the fire sources, are in qualitative agreement with TES observations from Dec 12th-15th, an apparently smaller event prior to the strong pyro-convection event starting Dec 14, 2006 discussed here and by Dirksen et al. (2009).

TES, MLS, and OMI observations of concentrations of the chemical tracer, CO, and the vertical aerosol loadings together with the meteorological wind fields provide evidence for transport pathways of pollutants produced in the December, 2006 Australian fires. However, the observations are too sparse and limited in time, which does not allow for a definitive description of the time evolution of the entire event. Although other A-train data (*e.g.*, vertical versus orbit track curtains of CloudSat ice-water content) provide complementary information, it is difficult to is difficult to correlate to the same transport event as observed with the Aura data. In addition to improved vertical resolution tracer profiles, better spatial and temporal coverage of the satellite dataset are required for the new generation of satellite instruments.

Acknowledgements

We would like to thank the helpful discussions on this work with Drs. Jennifer Logan, Jimmie Lopez, Line Jourdain, Lenny Pfister and O. Torres. Author J. H. Jiang thanks the support from the NASA ACMAP program. The research described in this paper was carried out at the Jet Propulsion Laboratory, California Institute of Technology, under a contract with the National Aeronautics and Space Administration. Funding at the University of Toronto was provided by the Natural Sciences and Engineering Research Council (NSERC) of Canada.

References

Andrea, M. and Merlet, P.: Emissions of trace gases and aerosols from biomass burning, Global Biogeochem. Cycles, 15, 955-966, 2001.

Arino, O., Plummer, S., and Casadio, S.: Fire Disturbance: the Twelve year time series of the ATSR World Fire Atlas, Proceedings of the ENVISAT Symposium 2007, SP-636, ESA, 2007.

Austin, R. T., A. J. Heymsfield, and G. L. Stephens (2009), Retrieval of ice cloud microphysical parameters using the CloudSat millimeter-wave radar and temperature, J. Geophys. Res., 114, D00A23, doi:10.1029/2008JD010049.

Badr, O. and Probert, S. D.: Carbon monoxide concentration in the Earth's atmosphere, Appl. Energy, 49, 99-143, 1994.

Bakwin, P. S., Tans, P. P., and Novelli, P. C.: Carbon monoxide budget in the Northern Hemisphere, Geophys. Res. Lett., 21, 433-436, 1994.

Beer, R., TES on the Aura Mission: Scientific Objectives, Measurements, and Analysis Overview, IEEE Trans. Geosci. Remote Sensing, 44, 1102- 1105, 2006.

Bey, I., D. J. Jacob, R. M. Yantosca, J. A. Logan, B. D. Field, A. M. Fiore, Q. Li, H. Liu, L. J. Mickley, and M. G. Schultz (2001), Global modeling of tropospheric chemistry with assimilated meteorology: Model description and evaluation, *J. Geophys. Res.*, 106, 23,073–23,089.

Boschetti, L., Roy, D., Barbosa, P., Boca, R., and Justice, C.: A MODIS assessment of the summer 2007 extent burned in Greece, Int. J. Rem. Sens., 29(8), 2433-2436, 2008.

Crutzen, P. and Andrea, M.: Biomass burning in the tropics: Impact on atmospheric chemistry and biogeochemical cycles, Science, 250, 1669-1678, 1990.

Dirksen, et al. (2009): An aerosol boomerang: rapid around-the-world transport of smoke from the December 2006 Australian forest fires observed from space, J. Geophys. Res., in press.

Edwards, D. P., Emmons, L. K., Hauglustaine, D. a., et al.: Observations of carbon monoxide and aerosols from the Terra satellite: Northern Hemisphere variability, J. Geophys. Res., 109, D24202, doi:10.1029/2004JD004727, 2004.

EFFIS Forest Fires in Europe 2007 report: Annual fire report, European Forest Fire Information System, JRC (http://effis.jrc.ec.europa.eu/reports/fire-reports), 2008.

Field, R. D., and S. S. P. Shen (2008), Predictability of carbon emissions from biomass burning in Indonesia from 1997 to 2006, J. Geophys. Res., 113, G04024, doi:10.1029/2008JG000694.

Freitas, S. R., et al.: Including the sub-grid scale plume rise of vegetation fires in low resolution atmospheric transport models, Atmos. Chem. Phys., 7, 3385-3398, 2007.

Fromm, M., Bevilacqua, R., Servanckx, R., Rosen, J., Thayer, J. P., Herman, J., and Larko, D.: Pyro-cumulonimbus injection of smoke to the stratosphere: Observations and impact of a super blowup in northwestern Canada on 3-4 August 1998, J. Geophys. Res., 110, D08205, doi:10.1029/2004JD005350, 2005.

Fromm, M., Tupper, A., Rosenfeld, D., Servranckx, R., and McRae, R.: Violent pyro-convective storm devastates Australia's capital and pollutes the stratosphere, Geophys. Res. Lett., 33, L05815, doi:10.1029/2005GL025161, 2006.

Guan, H., Chatfield, R. B., Freitas, S. R., Bergstrom, R. W., and Longo, K. M.: Modeling the effect of plume-rise on the transport of carbon monoxide over Africa with NCAR CAM, Atmos. Chem. Phys., 8, 6801-6812, 2008.

Hodzic, A., Vautard, R., Chepfer, H., Goloub, P., Menut, L., Chazette, P., Deuze, J. L., Apituley, A., and Couvert, P.: Evolution of aerosol optical thickness over Europe during the August 2003 heat wave as seen from CHIMERE model simulations and POLDER data, Atmos. Chem. Phys., 6, 1853-1864, 2006.

Hodzic, A., Madronich, S., Bohn, B., Massie, S., Menut, L., and Wiedinmyer, C.: Wildfire particulate matter in Europe during summer 2003: meso-scale modeling of smoke emissions, transport and radiative effects, Atmos. Chem. Phys., 7, 4043-4064, 2007.

Hyer, E. J., Allen, D. J., and Kasischke, E. S.: Examining injection properties of boreal forest fires using surface and satellite measurements of CO transport, J. Geophys. Res., 112, D18307, doi:10.1029/2006JD008232, 2007.

Justice, C. O., Giglio, L., Korontzi, S., Owens, J., Morisette, J., Roy, D., Descloitres, J., Alleaume, S., Petitcolin, f., and Kaufman, Y.: The MODIS fire products, Rmote Sens. Environ., 83, 244-262, 2002.

Kasischke, E. S. and Tretsky, M. R.: Recent changes in the fire regime across the North American boreal region-Spatial and temporal patterns of burning across Canada and Alaska, Geophys. Res. Lett., 33, L09703, doi:10.1029/2006GL025677.

Khalil, M. A. K. and Rasmussen, R. A.: Carbon monoxide in the Earth's atmosphere: Indications of a global increase, Nature, 332, 242-245, 1988.

Khalil, M. A. K.,and Rasmussen, R. A.: Global decrease in atmospheric carbon

monoxide concentration, Nature, 370, 639-641, 1994.

Lamarque, J.-F., Edwards, D. P., Emmons, L. K., et al.: Identification of CO plumes from MOPIT data: application to the August 2000 Idaho-Montana forest fires, Geophys. Res. Lett., 30(13), 1688, doi:10.1029/2003GL017503, 2003.

Lapina, K., Honrath, R. E., Owen, R. C., ValMartin, M., and Pfister, G.: Evidence of significant large-scale impacts of boreal fires on ozone levels in midlatitude Northern Hemisphere free troposphere, Geophys. Res. Lett., 33, L10815, doi:10.1029/2006GL025878. 2006.

Liousse, C., Penner, J. E., Chuang, C., Walton, J. J., Edleman, H., and Cachier, H.: A global three-dimensional model study of carbonaceous aerosols, J. Geophys. Res., 101(D14), 19411-19432, 1996.

Livesey, N.J., M.D. Fromm, J.W. Waters, G.L. Manney, M.L. Santee, and W.G. Read, Enhancements in lower stratospheric CH_3CN observed by UARS MLS fillowing boreal forest fires, J. Geophys. Res. 109, D06308, doi:10.1029/2003JD004055, 2004.

Livesey, N. J., et al.: Validation of Aura Microwave Limb Sounder O3 and CO observations in the upper troposphere and lower stratosphere, J. Geophys. Res. 113, D15S02, doi:10.1029/2007JD008805, 2008.

Logan, J. A., Prather, J. M., Wofsy, S. C., and McElroy, M. B.: Tropospheric chemistry:

A global perspective, J. Geophys. Res., 86, 710-7254, 1981.

Logan, J. A., I. A. Megretskaia, R. Nassar, L. T. Murray, L. Zhang, K. W. Bowman, H. M Worden, M. Luo (2008), Effects of the 2006 El Niño on tropospheric composition as revealed by data from the Tropospheric Emission Spectrometer (TES), Geophys. Res. Lett., 35, L03816, doi:10.1029/2007GL031698.

Luo, M., Rinsland, C. P., Rodgers, C. D., Logan, J. A., Worden, H., Kulawik, S., Eldering, A., Goldman, A., Shephard, M. W., Gunson, M., and Lampel, M.: Comparison of carbon monoxide measurements by TES and MOPITT: Influence of a priori data and instrument characteristics on nadir atmospheric species retrievals, J. Geophys. Res., 112, D09303, doi:10.1029/2006JD007663, 2007.

McMillan, W. W., Warner, J. X., McCourt Comer, M., et al.: AIRS views transport from 12 to

22 July 2004 Alaskan/Canadian fires: Correlation of AIRS CO and MODIS AOD with forward trajectories and comparison of AIRS CO retrievals with DC-8 in situ measurements during INTEX-A/ICARTT, J. Geophys. Res., 113, D20301, doi:10.1029/2007JD009711, 2008.

Nassar, R., Logan, J. A., Megretskaia, I. A., Murray, L. T., Zhang, L., and Jones, D. B. A.: Analysis of tropospheric ozone, carbon monoxide and water vapor during the 2006 El Nino using TES observations and the GEOS-Chem model, J. Geophys. Res., doi:10.1029/2009JD011760, 2009.

Novelli, P. C., Masarie, K. A., Tans, P. P., and Lang, P. M.: Recent changes in atmospheric carbon monoxide, Science, 263, 1587-1590, 1994.

Olivier, J. G. J. and Berdowski, J. J. M.: Global emissions sources and sinks in: Climate System, edited by: Berdowski, J., Guicherit, R., and Heij, B. J., 33-78, A. A. Balkema Publishers/Swets & Zeitlinger Publishers, Lisse, The Netherlands, ISBN 90 5809 255 0, 2001..

Parrish, D. D., et al.: Decadal change in carbon monoxide to nitrogen oxide ratio in U.S. vehicular emissions, J. Geophys. Res., 107(D12), 4140, doi:10.1029/2001JD000720, 2002.

Rinsland, C. P., M. Luo, M. W. Shephard, C. Clerbaux, C. Boone, P. F. Bernath, L. Chiou, P. F. Coheur (2008), Tropospheric emission spectrometer (TES) and Atmospheric Chemistry Experiment (ACE) measurements of tropospheric chemistry in tropical southeast Asia during a moderate El Niño in 2006, J. Quant. Spectrosc. Radiat. Trans., 109, 1931-1942, doi:10.1016/j.jqsrt.2007.12.020.

Rodgers, C. D.: Information content and optimization of high spectral resolution remote measurements, Adv. Space Res., 21(31), 361-367, 1998.

Seiler, W. and Crutzen, P. J.: Estimates of gross and net fluxes of carbon between the biosphere and the atmosphere from biomass burning, Clim. Change, 2, 207-247, 1980.

Schoeberl,M. R., and S. Talabac (2006), The SensorWeb: Afuture technique for science return, in Observing Systems for Atmospheric Composition, edited by G. Visconti et al., pp. 203–206, Springer, New York.

Stammes, P., Tilstra, L. G., Braak, R., Graaf, M. de., and Aben, E. A. A.: Estimate of Solar Radiative Forcing by Polluted Clouds Using OMI and SCIAMACHY Satellite Data, in *AIP Conference Proceedings*, 1100, edited by T. Nakajima and M. A. Yamasoe, pp. 577-580, doi:10.1063/1.3117051.

Szopa, S., Hauglustaine, D. A., and Ciais, P.: Relative contributions of biomass burning

emissions and atmospheric transport to carbon monoxide interannual variability, Geophys. Res. Lett., 34, L18810, doi:10.1029/2007GL030231, 2007.

Thompson, A. M., Pickering, K. E., Dickerson, R. R., Ellis, W. G., Jacob, D. J., Scala, J. R., Tao, W., McNamara, D. P., and Simpson, J.: Convective transport over the central United States and its role in regional CO and ozone budgets, J. Geophys. Res., 99, 18703-18711, 1994.

Torres, O., A. Tanskanen, B. Veihelmann, C. Ahn, R. Braak, P. K. Bhartia, P. Veefkind, and P. Levelt (2007), Aerosols and surface UV products from Ozone Monitoring Instrument observations: An overview, J. Geophys. Res., 112, D24S47, doi:10.1029/2007JD008809.

Turquety, S., et al.: Inventory of boreal fire emissions for North America in 2004: Importance of peat burning and pyroconvective injection, J. Geophys. Res., 112, D12S03, doi:10.1029/2006JD007281, 2007.

van der Werf, G. R., Randerson, J. T., Giglio, L., Collatz, G. J., Kasibhatla, P. S., and Arellano, Jr., A. F.: Interannual variability in global biomass burning emissions from 1997 to 2004, Atmos. Chem. Phys., 6, 3423-3441, 2006.

van der Werf, G. R., J. Randerson, L. Giglio, N. Gobron, and H. Dolman (2008), Climate controls on the variability of fires in the tropics and subtropics, *Global Biogeochem. Cycles*, 22, GB3028, doi:10.1029/2007GB003122.

van Donkelaar, A., et al. (2008), Analysis of aircraft and satellite measurements from the Intercontinental Chemical Transport Experiment (INTEX-B) to quantify long-range transport of East Asian sulfur to Canada, *Atmos. Chem. Phys.*, 8, 2999–3014.

Waters, J.W. et al., The Earth Observing System Microwave Limb Sounder (EOS MLS) on the Aura satellite, IEEE Trans. Geosci. Remote Sensing, 44, no. 5, 2006.

Wotawa, G., Novelli, P., Trainer, M., and Granier, C.: Inter-annual variability of summertime CO concentrations in the Northern Hemisphere explained by boreal forest fires in Northern America and Russia, Geophys. Res. Lett., 28(24), 4575-4578, 2001.

Yurganov, L. N., Grechko, E. I., and Dzhola, A. V.: Variations in carbon monoxide density in the total atmospheric column over Russia between 1970 and 1995: Upward trend and disturbances attributed to the influence of volcanic aerosols and forest fires, Geophys. Res. Lett., 24(10), 1231-1234, 1997.

Yurganov, L. N., et al.: A quantitative assessment of the 1998 carbon monoxide emission

anomaly in the Northern Hemisphere based on total column and surface concentration measurements, J. Geophys. Res., 109, D15305, doi:10.1029/2004JD004559, 2004.

Yurganov, L. N., W. W. McMillan, A. V. Dzhola, E. I. Grechko, N. B. Jones, G. R. van der Werf (2008), Global AIRS and MOPITT CO measurements: Validation, comparison, and links to biomass burning variations and carbon cycle, J. Geophys. Res., 113, D09301, doi:10.1029/2007JD009229.

Figure 1

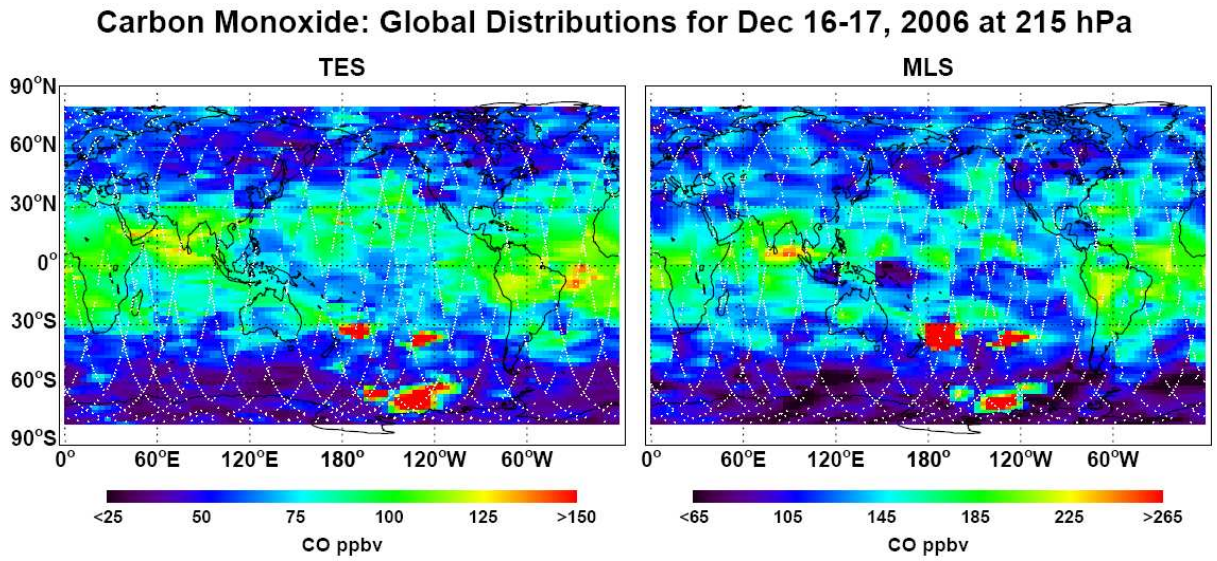
Carbon Monoxide: Global Distributions for Dec 16-17, 2006 at 215 hPa
TES
MLS
90°N
60°N
30°N
0°
30°S
60°S
90°S
0°
60°E
120°E
180°
120°W
60°W
<25
50
75
100
125
>150
CO ppbv
<65
105
145
185
225
>265
CO ppbv

Figure 2

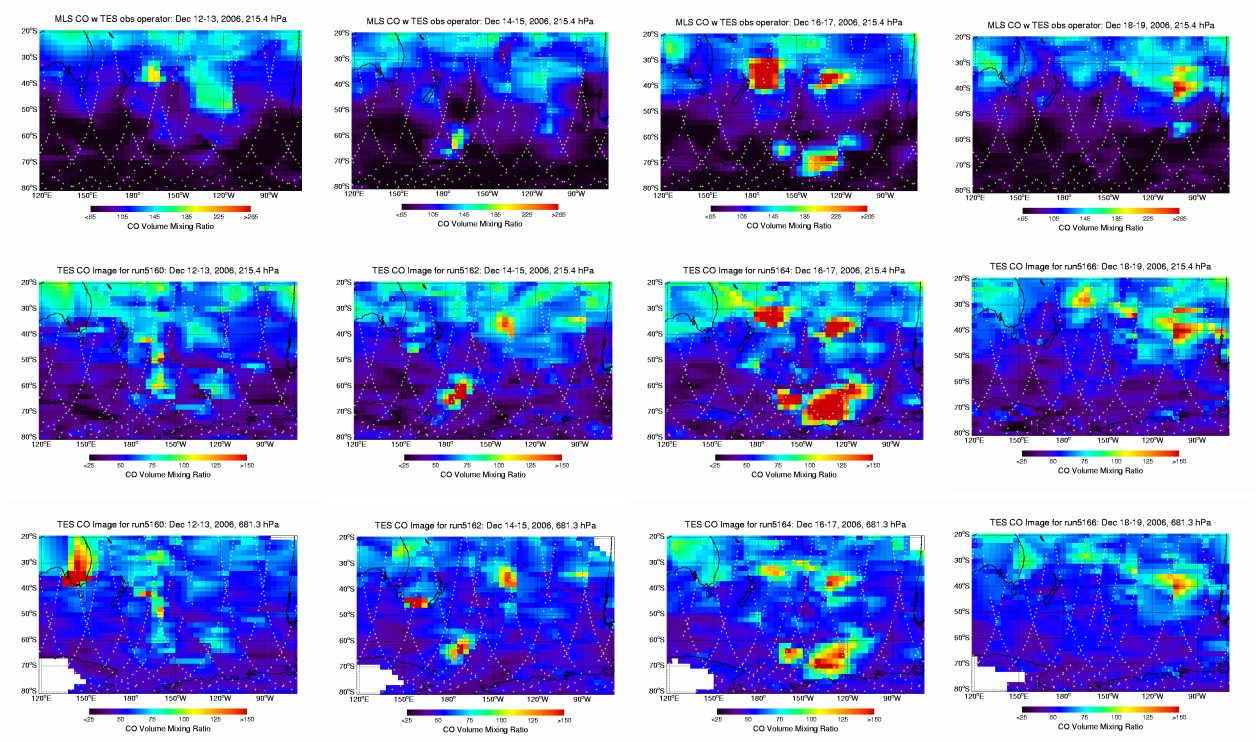
MLS CO w TES obs operator: Dec 12-13, 2006, 215.4 hPa
MLS CO w TES obs operator: Dec 14-15, 2006, 215.4 hPa
MLS CO w TES obs operator: Dec 16-17, 2006, 215.4 hPa
MLS CO w TES obs operator: Dec 18-19, 2006, 215.4 hPa
TES CO Image for run5160: Dec 12-13, 2006, 215.4 hPa
TES CO Image for run5162: Dec 14-15, 2006, 215.4 hPa
TES CO Image for run5164: Dec 16-17, 2006, 215.4 hPa
TES CO Image for run5166: Dec 18-19, 2006, 215.4 hPa
TES CO Image for run5160: Dec 12-13, 2006, 681.3 hPa
TES CO Image for run5162: Dec 14-15, 2006, 681.3 hPa
TES CO Image for run5164: Dec 16-17, 2006, 681.3 hPa
TES CO Image for run5166: Dec 18-19, 2006, 681.3 hPa
CO Volume Mixing Ratio

Figure 3

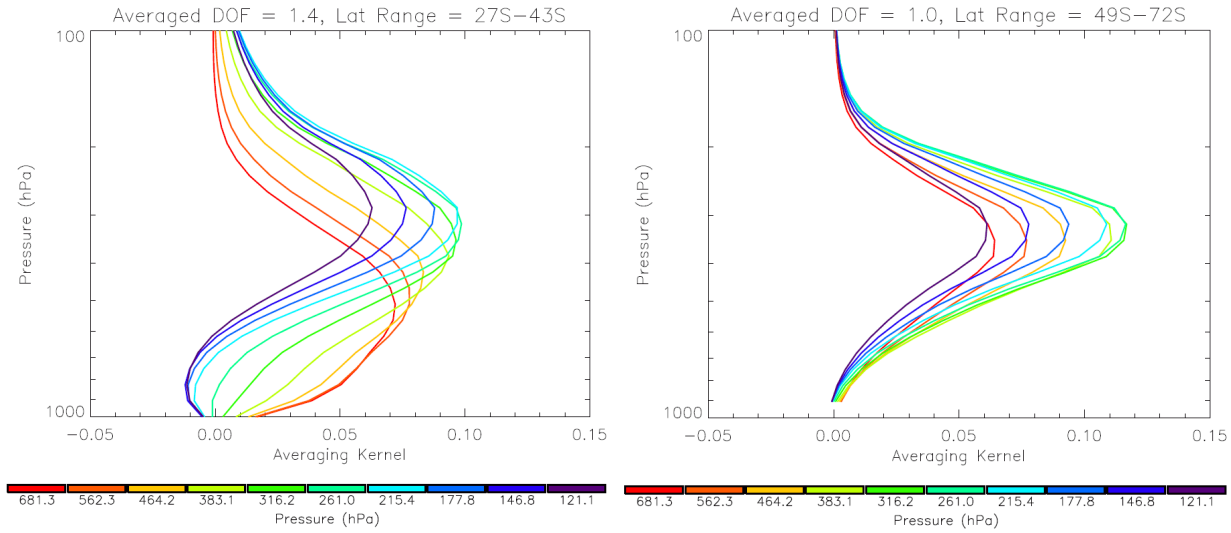
Averaged DOF = 1.4, Lat Range = 27S–43S
Averaged DOF = 1.0, Lat Range = 49S–72S
Pressure (hPa)
100
1000
−0.05
0.00
0.05
0.10
0.15
Averaging Kernel
681.3
562.3
464.2
383.1
316.2
261.0
215.4
177.8
146.8
121.1
Pressure (hPa)

Figure 4

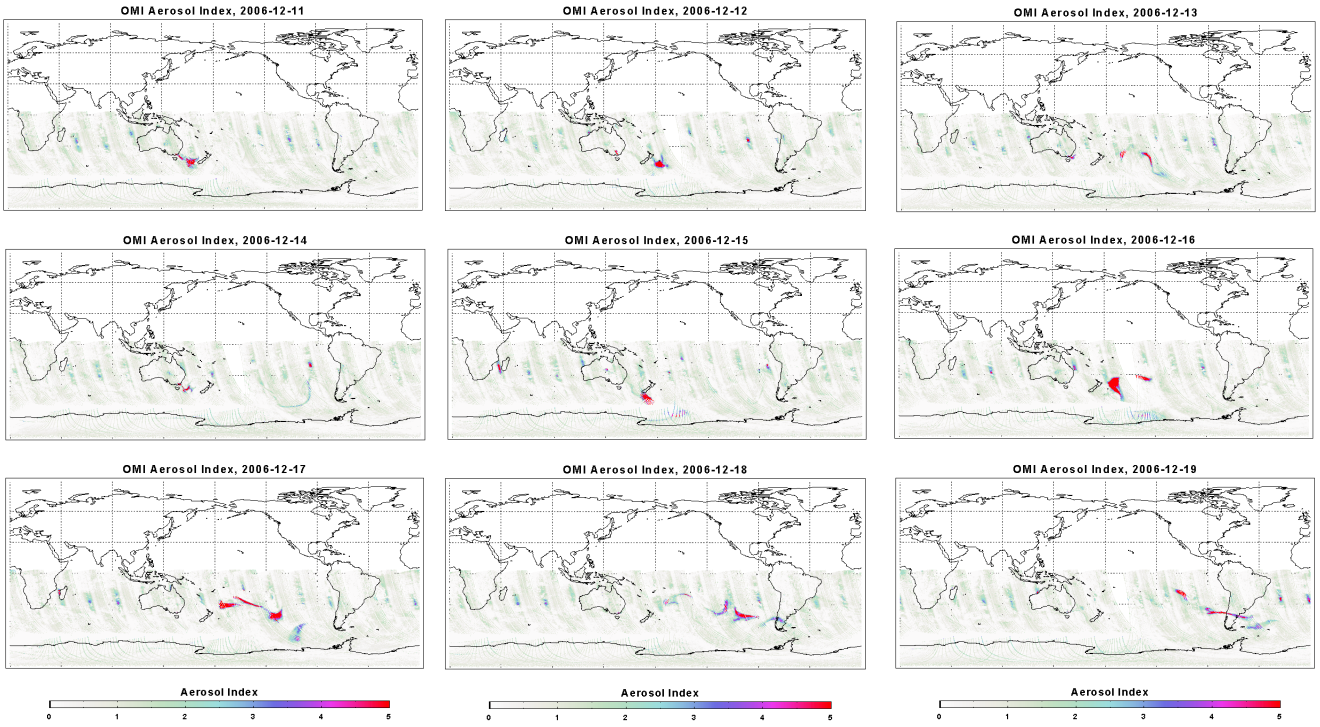
OMI Aerosol Index, 2006-12-11
OMI Aerosol Index, 2006-12-12
OMI Aerosol Index, 2006-12-13
OMI Aerosol Index, 2006-12-14
OMI Aerosol Index, 2006-12-15
OMI Aerosol Index, 2006-12-16
OMI Aerosol Index, 2006-12-17
OMI Aerosol Index, 2006-12-18
OMI Aerosol Index, 2006-12-19
Aerosol Index
0 1 2 3 4 5
Aerosol Index
0 1 2 3 4 5
Aerosol Index
0 1 2 3 4 5

Figure 5

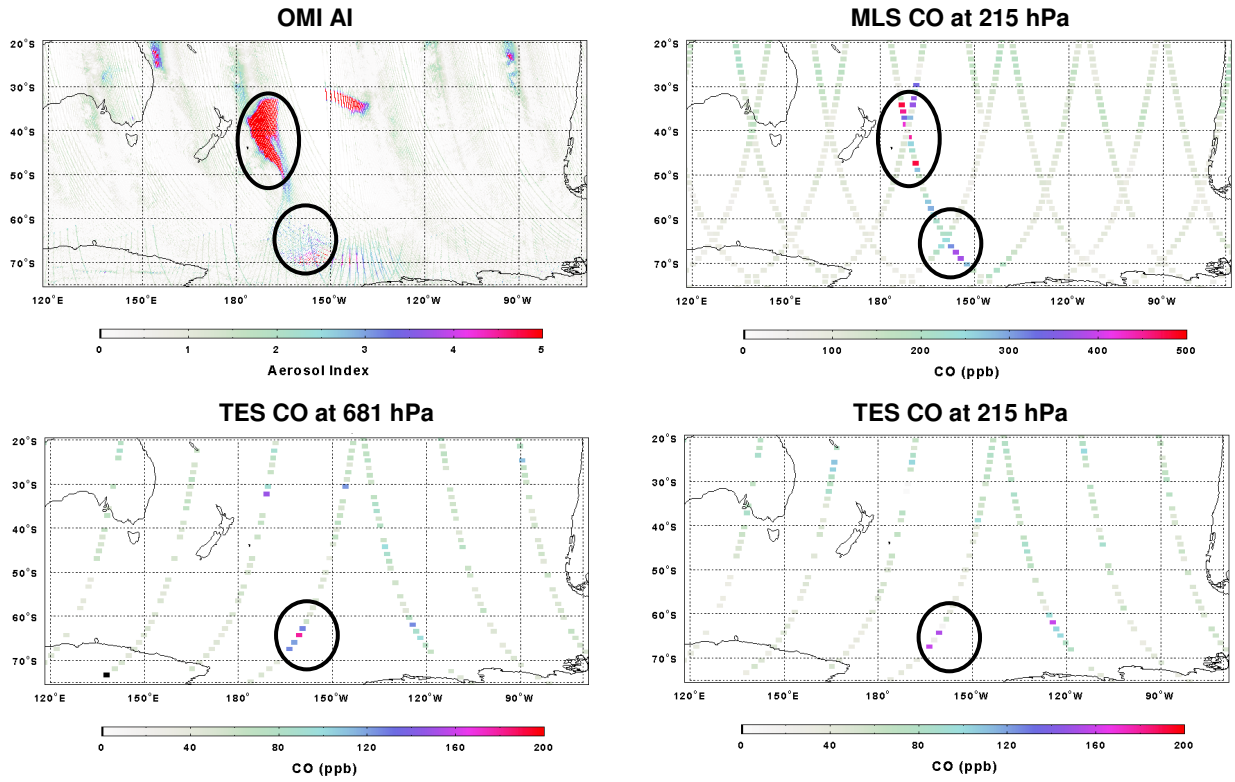
OMI AI
20°S
30°S
40°S
50°S
60°S
70°S
120°E
150°E
180°
150°W
120°W
90°W
0
1
2
3
4
5
Aerosol Index
MLS CO at 215 hPa
0
100
200
300
400
500
CO (ppb)
TES CO at 681 hPa
0
40
80
120
160
200
CO (ppb)
TES CO at 215 hPa
CO (ppb)

Figure 6

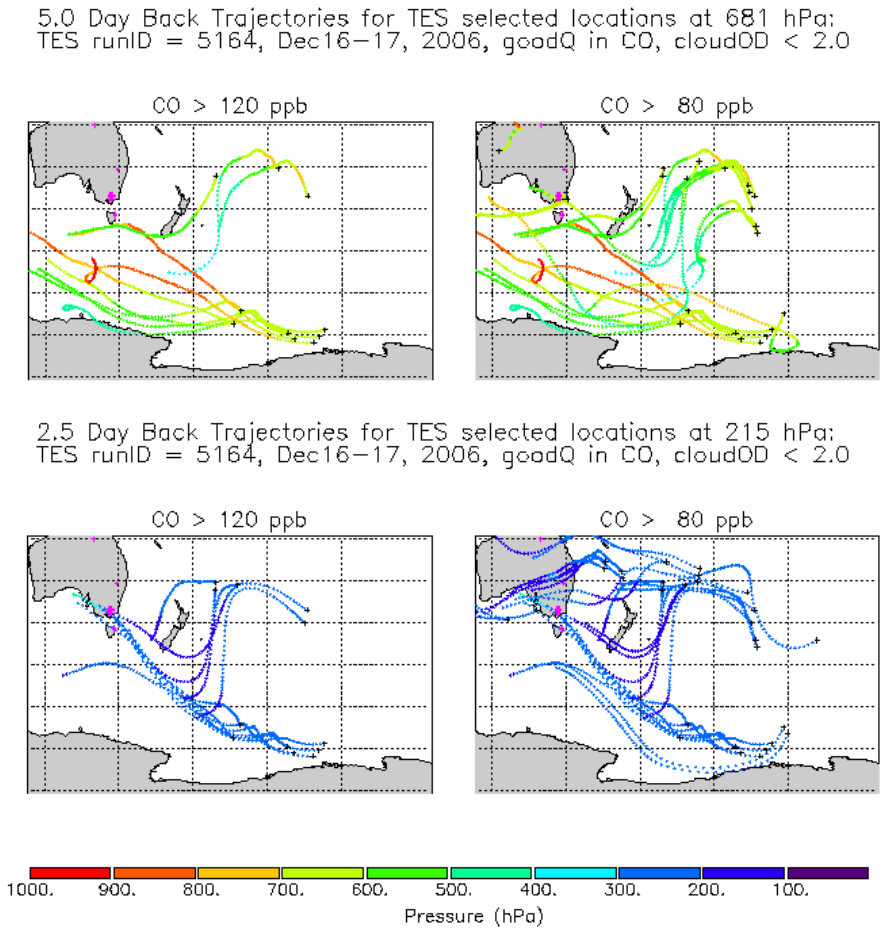
5.0 Day Back Trajectories for TES selected locations at 681 hPa:
TES runID = 5164, Dec16–17, 2006, goodQ in CO, cloudOD < 2.0
CO > 120 ppb
CO > 80 ppb
2.5 Day Back Trajectories for TES selected locations at 215 hPa:
TES runID = 5164, Dec16–17, 2006, goodQ in CO, cloudOD < 2.0
CO > 120 ppb
CO > 80 ppb
1000.
900.
800.
700.
600.
500.
400.
300.
200.
100.
Pressure (hPa)

Figure 7

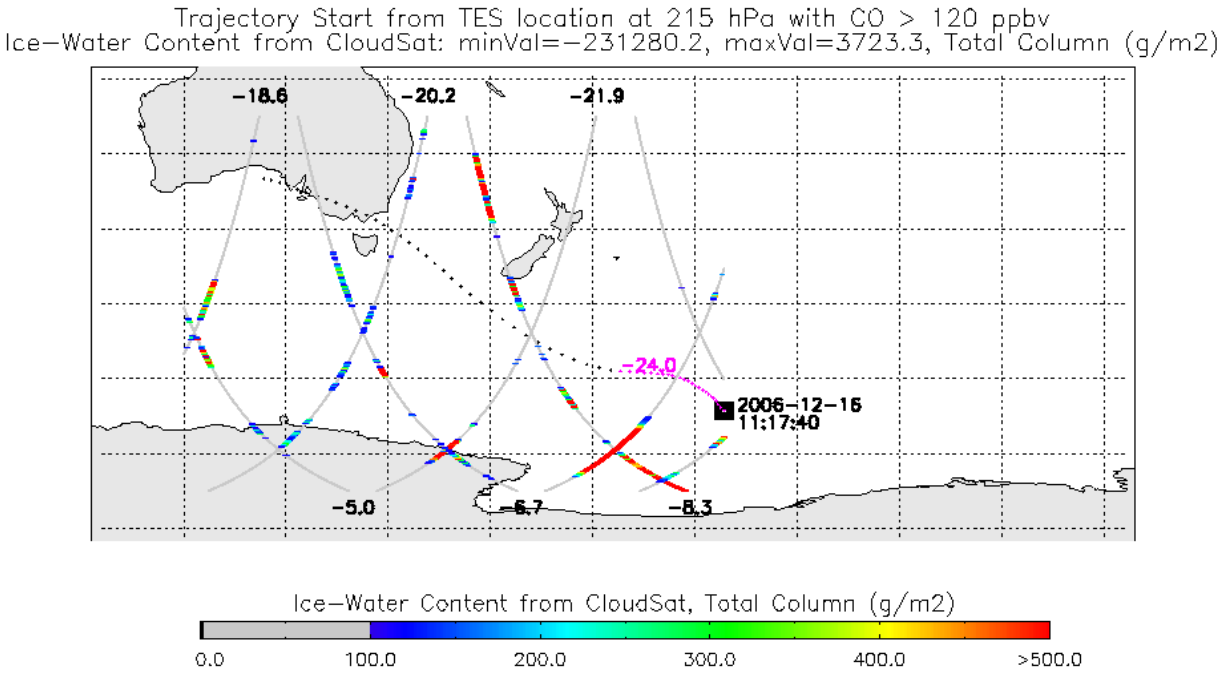
Trajectory Start from TES location at 215 hPa with CO > 120 ppbv
Ice–Water Content from CloudSat: minVal=–231280.2, maxVal=3723.3, Total Column (g/m2)
–18.6
–20.2
–21.9
–24.0
2006–12–16
11:17:40
–5.0
–6.7
–8.3
Ice–Water Content from CloudSat, Total Column (g/m2)
0.0
100.0
200.0
300.0
400.0
>500.0

Figure 8

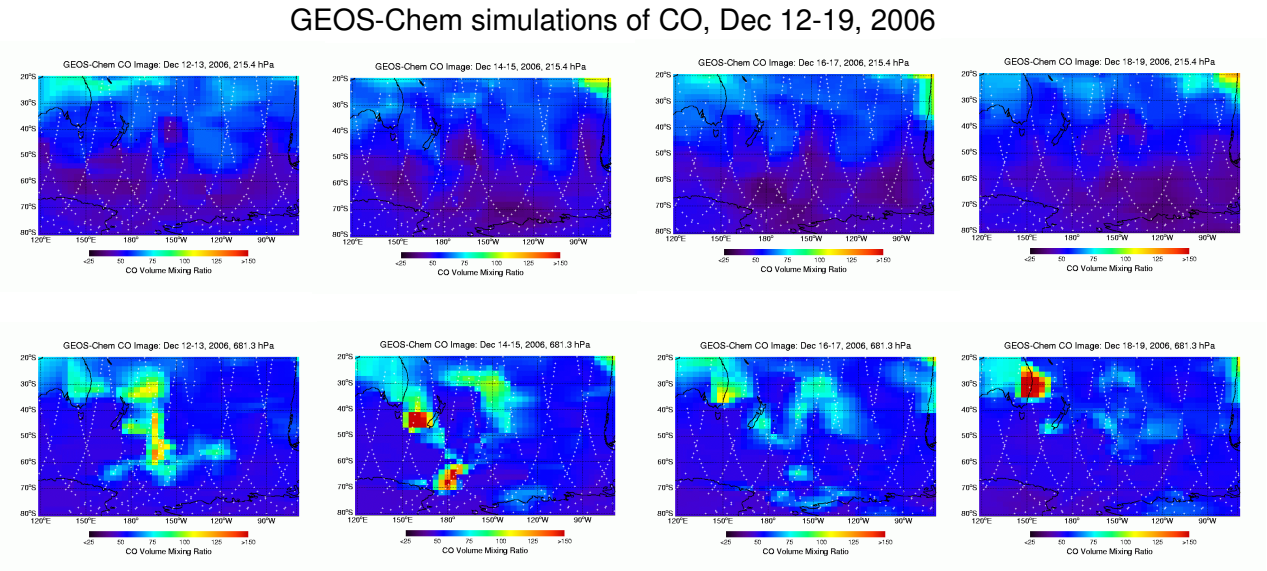
GEOS-Chem simulations of CO, Dec 12-19, 2006
GEOS-Chem CO Image: Dec 12-13, 2006, 215.4 hPa
GEOS-Chem CO Image: Dec 14-15, 2006, 215.4 hPa
GEOS-Chem CO Image: Dec 16-17, 2006, 215.4 hPa
GEOS-Chem CO Image: Dec 18-19, 2006, 215.4 hPa
GEOS-Chem CO Image: Dec 12-13, 2006, 681.3 hPa
GEOS-Chem CO Image: Dec 14-15, 2006, 681.3 hPa
GEOS-Chem CO Image: Dec 16-17, 2006, 681.3 hPa
GEOS-Chem CO Image: Dec 18-19, 2006, 681.3 hPa
CO Volume Mixing Ratio

Captions

Figure 1. Left panel: TES retrievals of CO from global survey observations taken December 16th-17th, 2006 at 215 hPa. Right panel: MLS retrievals of CO at 215 hPa from the profiles closest to those of TES in location and time. The white marks are TES profile geolocations or those of MLS.

Figure 2. Top row: MLS CO at 215 hPa (with TES observation operator applied); Mid row: TES CO at 215 hPa; Bottom row: TES CO at 681 hPa. The four columns: TES Global Surveys of December 12th-13th, Dec.14-15, Dec.16-17, and December 18th-19th, 2006. The location of the TES and MLS footprints are marked by the white symbols with the remainder of the distribution determined through spatial interpolation.

Figure 3. Mean TES Averaging Kernels of selected observations, December 12th-19th, 2006. Profile selection criteria: cloudOD <2.0, CO > 120 ppb at 215 hPa or 681 hPa. Profiles used for the left panel are in latitude band of 27 ^{o} S - 43 ^{o} S (num of profiles for averaging = 15). Profiles used for the right panel are in latitude band of 49^{o} S – 72^{o} S (num of profiles for averaging = 12).

Figure 4. OMI aerosol index (AI) in Southern Hemisphere for December 11th-19th, 2006.

Figure 5. Illustrations of OMI AI, MLS CO at 215 hP, and TES CO at 681 hPa and 215 hPa for December 16th, 2006. Data in the circles indicates matches of enhanced AI and CO values.

Figure 6. Back trajectories starting at selected TES profile locations (marked by black cross symbols), December 16th-17th, 2006. Top panels are the five day trajectories starting at 681 hPa, for CO > 120 ppbv (left) and CO > 80 ppbv (right), respectively. Bottom panels are the 2.5 day, trajectories starting at 215 hPa, for CO > 120 ppbv (left) and CO > 80 ppbv (right), respectively. MODIS 8-day Climate Modeling fire pixel > 50 are marked by magenta dots.

Figure 7. A backward trajectory started from a TES profile location (dark square). The trajectory is represented by the black dotted curve, and the overlaid magenta curve represents the trajectory portion of 0 to -24 hrs. The light-gray tracks indicate the location of the CloudSat orbits with colored Ice-Water content total column measurements. The CloudSat overpass times relative to the TES observation times (or zero) are in black for the corresponding orbit tracks.

Figure 8. GEOS-Chem simulations of CO sampled at the TES profile footprints and times, December 12th-19th, 2006. Top row: GEOS-Chem CO at 215 hPa; Bottom row: GEOS-Chem CO at 681 hPa. The four columns: TES Global Surveys of December 12th-13th, 14th-15th, 16th-17th, and 18th-19th, 2006.